Earth, Planets and Space

FULL PAPER

Open Access

Source mechanisms and triggering process for the April 12th and 13th, 2014 earthquake doublet in the Solomon Islands

Calvin Luiramo Qwana[1*], Masatoshi Miyazawa[2] and James Mori[2]

Abstract

Mw 7.6 and Mw 7.4 earthquakes occurred 16 h apart on April 12 and April 13, 2014, at depths of 15 km and 35 km, respectively, southwest of Makira Island (San Cristobal) in the Solomon Islands. We study the source mechanisms to investigate the interrelation between the two events, and to investigate why the Solomon Islands have a historically high rate of doublet earthquakes. Teleseismic P waveform data for both events were used to obtain the slip distributions for the two earthquakes by a finite fault slip inversion method. The Mw 7.6 event is an east–west left-lateral strike slip, where the maximum slip is observed 8–24 km east of the hypocenter. The Mw 7.4 earthquake is a thrust event with north and south-dipping nodal planes. The fault plane is not clear from the aftershock distribution, but the north-dipping plane considered to be the likely fault plane because of the simpler slip distribution compared to the south-dipping plane. The static Coulomb failure stress changes caused by the first earthquake were calculated in the region of the second earthquake. The results show that there was a + 48.59 kPa change at the hypocenter for the assumed north-dipping plane and + 18.24 kPa for the assumed south-dipping plane of the Mw 7.4 event. The temporal pattern of aftershocks shows a possible rate increase of stress prior to the occurrence of the Mw 7.4 events, which may also contribute to the triggering of the second event by static Coulomb Stress changes. We propose a model that supports the geological complexity of the region that may encourage such doublet events.

Keywords Solomon Islands, Doublet earthquakes, Aftershocks, Coulomb stress changes, Teleseismic waveform inversion, Slip models, Asperity

*Correspondence:
Calvin Luiramo Qwana
qwana.luiramo.35x@st.kyoto-u.ac.jp
Full list of author information is available at the end of the article

Graphical Abstract

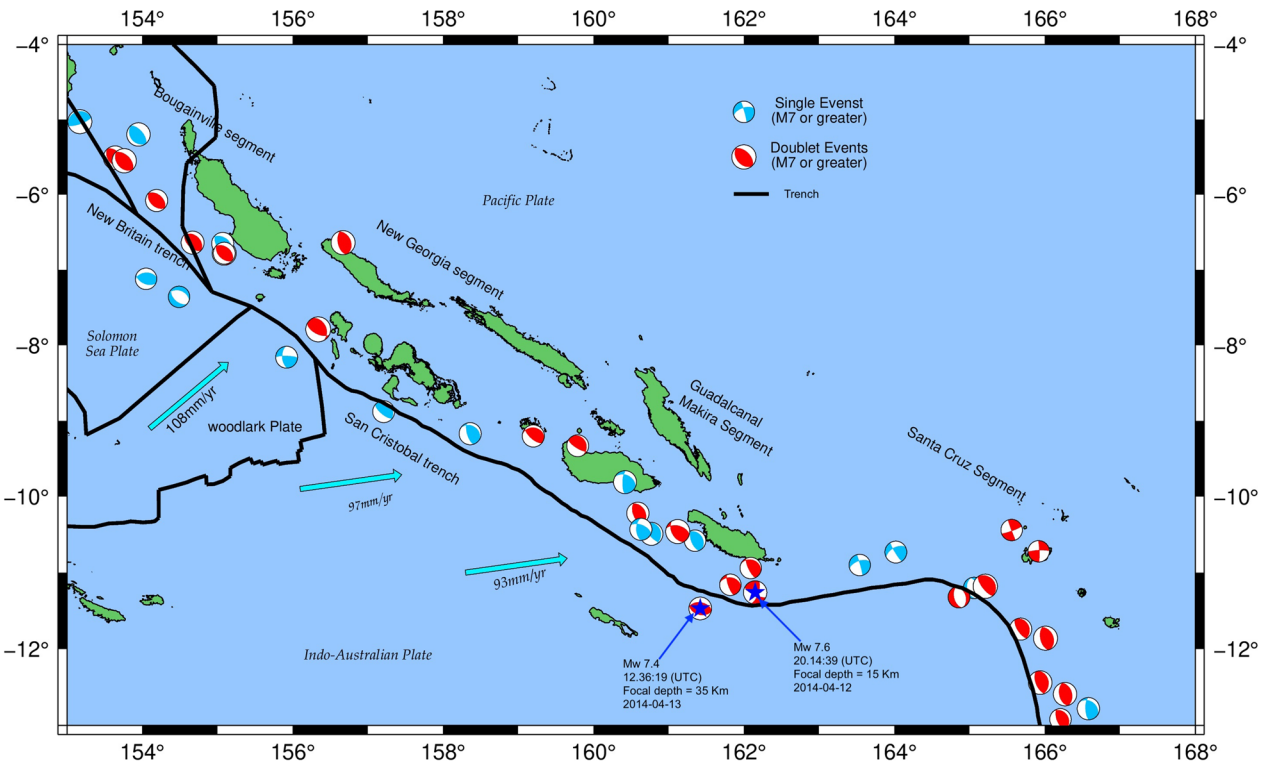

Introduction

The Solomon Islands region is characterized by a complexity of tectonic microplates, which is a result of the convergence of the Indo-Australian and Pacific plates. The Indo-Australia plate is moving northeast at an average rate of ~ 6 cm/year with variations along the boundaries up to ~ 13 cm/year. The archipelago is bounded by two trench systems, the Vitiaz trench (locally named the North Solomon trench) to the northeast and the New Britain–San Cristobal trench to the southwest. In the northwest, the bathymetry plunges to a depth of ~ 4500 m parallel to the Vitiaz trench and joins the San Cristobal trench in the southeast. Tectonic models of the region reflect the complex dynamic evolution and terrain accretion processes that form the present-day Solomon Island Archipelago (Petterson et al. 1999). The region is well known for a doublet or multiple earthquakes that are defined by Lay and Kanamori 1980 as two or more events of similar magnitude where their occurrences are separated closely in time compared to the recurrence time and in space within about a fault length. The mechanism responsible for triggering of these sequences is still not well understood, although multiple earthquakes are thought to indicate heterogeneity in the faulting process (Lay and Kanamori 1980; Wesnousky et al. 1986). In the Solomon Island region, these events often occurred as pairs (Lay and Kanamori 1980; Schwartz et al. 1989; Xu and Schwartz 1993) with small separations in time (hours to days) and space of 50–100 km. Doublets and multiple events also occur in the adjacent region of Papua New Guinea to the northeast of this study area (e.g., Park and Mori 2007) and further west in Irian Jaya (e.g., Poiata et al. 2010), but far less frequently compared to the Solomon Islands region. A better understanding of the triggering process which promotes occurrences of doublet earthquakes in this unique region would offer clarification of the physical mechanism and help explain why the Solomon Islands region has such a high rate of doublet earthquakes.

The Solomon Islands region is one of the most seismically active regions on the Pacific Rim of Fire, and since 1950 there were 43 events of magnitude Mw 7.0 or greater that occurred within 500 km of the capital Honiara (Fig. 1).

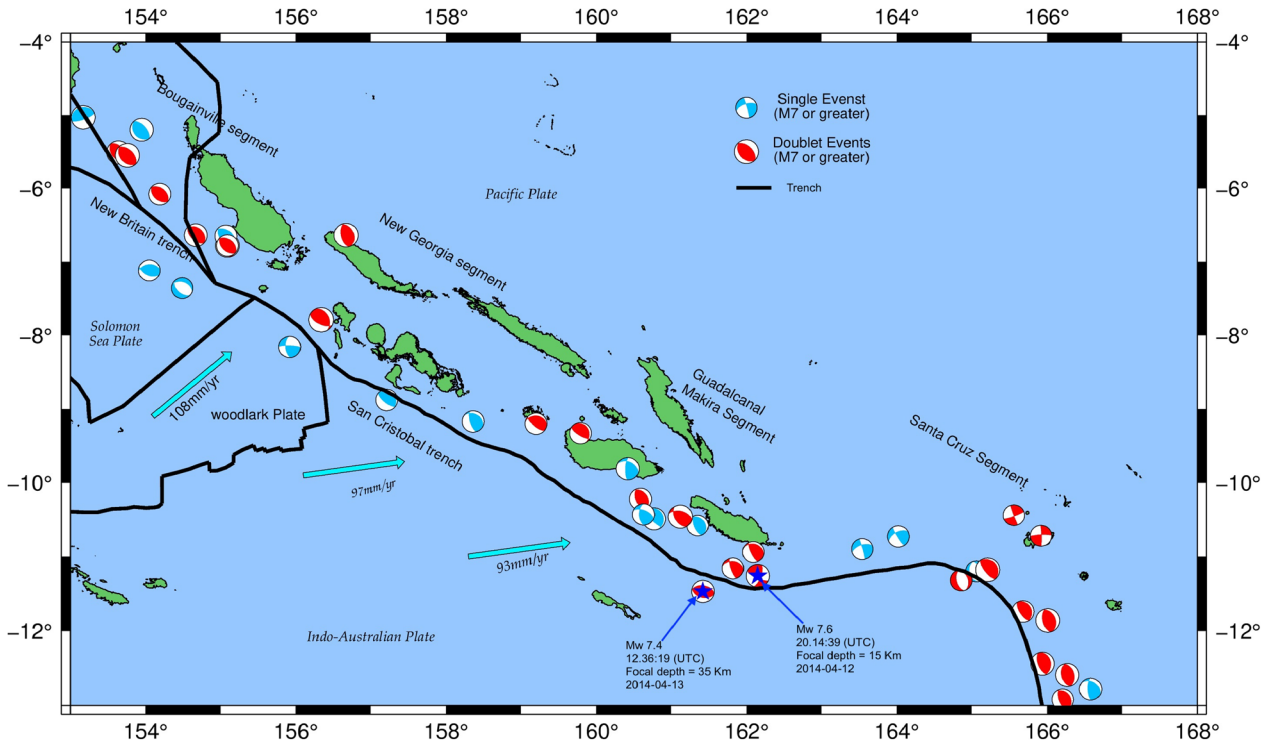

Fig. 1 Mw 7.0 or greater earthquakes that occurred along the Indo-Australia and Pacific Plate boundary since 1950 for the Solomon Islands region**.** The moment tensors with stars indicate the events in this study (Mw 7.6, and Mw 7.4). The blue beachballs indicate the focal mechanisms of single earthquake events and the red beachballs indicate earthquake doublets or multiplets. The light blue arrows indicate the Indo-Australia and Pacific Plate rates relative to the plate boundaries which are indicated by the thick black lines. Focal mechanisms are from the Global CMT Catalog data, Ekström et al. 2012)

While it is a common assumption that the occurrence of major earthquakes rearranges the local stress field, which can lead to triggering of other large earthquakes on nearby faults, much still remains to fully understand the underlying mechanics that control the timing and locations of the triggered events. This study focuses on a doublet earthquake sequence that occurred on April 12, 2014 at 20.14.39 GMT (Mw 7.6) and April 13, 2014 at 12.36.19 GMT (Mw 7.4). To study the relation between the first Mw 7.6 earthquake and second Mw 7.4 earthquake, we first determined the slip distributions for the two earthquakes, then using the derived fault models, we calculated the static stress changes from the first event for the region of the second earthquake. Furthermore, we compare the rupture process for the two earthquakes with their aftershock patterns to study the spatial distribution patterns. The triggering potential, timing, and location of the Mw 7.4 earthquake and aftershocks provide important information about the heterogeneity of the fault and relationship between the two earthquakes.

Slip distributions for two earthquakes

We first determine the slip distributions for the Mw 7.6 and Mw 7.4 earthquakes using teleseismic P-wave data from the same 21 stations of the Global Seismic Network (GSN) stations located within the distance range of 30 degrees to 90 degrees. Stations were chosen to have a good azimuthal coverage as shown in Fig. 2. The broadband vertical (BHZ) components were band-passed filtered between 0.01 Hz and 0.10 Hz and corrected for the instrument response. We used the program of Kikuchi and Kanamori (1991) to invert the teleseismic data for the slip distributions of the two earthquakes. The synthetic green functions were calculated using the global velocity model IASPEI91 (Kennett and Engdahl 1991). For the inversion process, the P-wave data and model synthetics were sampled at 0.2 s.

Mw 7.6 earthquake on April 12

The Mw 7.6 event on April 12, 2014, has a strike-slip mechanism with nearly north–south and east–west striking nodal planes. The elongated distribution of aftershocks is in a generally east–west direction suggesting that the east–west striking nodal plane is likely the fault

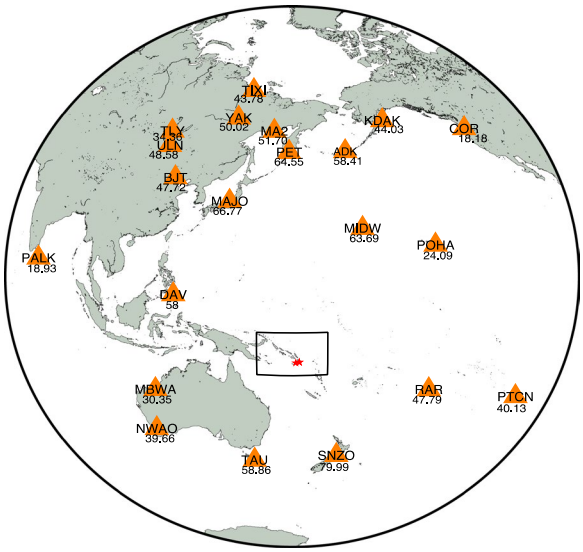

Fig. 2 Station distribution used for the waveform inversions for the Mw 7.6 April 12 and Mw 7.4 April 13, 2014, events, shown by the red stars. The rectangle shows the Solomon Islands region

plane. For the inversion, we first assumed a fault that has a strike of 116° and dip of 74° from the focal mechanisms calculated by assuming a point source. For the slip inversion, the fault plane has a length of 80 km and a width of 40 km with a subfault of size 8 × 10 km. Several different sizes for the fault were tested with lengths of 50–100 km. We chose the size that best contained the slip distribution for the waveform duration of 60 s. We tried several hypocentral depths to test the value that produced the best fit to the waveforms (Table 1) and found the best-fitting hypocenter was at a depth of 15 km. The better fit of the model to the data for the shallower depths is due to the better fit in the first 10–30 s of the waveforms which are controlled by the timing of the depth phases (Table 2).

The epicenter is set to 11.270°S 162.148°E. The fit of teleseismic waveforms is not very sensitive to the epicenter, because the first arrivals of the model and observed data are aligned. We also tested various rupture velocities from 2.0 to 3.0 km/s. The results for these teleseismic data are not very sensitive to the rupture velocity, however, the optimal rupture velocity was 2.5 km/s.

The results for the teleseismic waveform inversion show a fairly simple slip distribution that is distributed over a length of about 80 km in Fig. 3. The maximum slip of 2–3 m is located approximately 8–16 km east of the hypocenter. The source time function shows several pulses over a duration of about 60 s with a total seismic moment of $Mo = 3.33 \times 10^{20} Nm$. The waveform match between the observed (bold black lines) and calculated seismograms (thin brown lines) is shown on the right of Fig. 3.

Our slip distribution is rather similar in shape and size to the solution from USGS (https://earthquake.usgs.gov/earthquakes/eventpage/usc000phx5/finite-fault), however, the location of the area of large slip relative to the hypocenter is different. This relative location difference is probably due to differences in the way initial arrivals are determined for each station. Our hypocentral depth is somewhat different from the USGS depth, although the difference is smaller than the vertical grid size used in our inversion. We also carried out the waveform inversion for the north–south nodal plane. However, the fit to the waveforms was significantly worse than for the east–west plane (Fig. 4), confirming the choice of the east–west fault plane from the aftershock distribution. The variance was 0.1853 for the east–west nodal plane versus 0.1958 for the north–south nodal plane.

Mw 7.4 earthquake on April 13

The Mw 7.4 event on April 13, 2014, shows a thrust mechanism with north and south-dipping nodal planes.

Table 1 Testing of various depth for the hypocenter for the determined focal depth with the smallest variance is for 15 km

Focal depths (km)	10	15	20	25	30	35
Variance	0.1854	0.1853	0.1970	0.2067	0.2095	0.2204
Mw	7.59	7.61	7.60	7.66	7.65	7.68

Table 2 Testing of various depth for the hypocenter for the determined focal depth with the smallest variance is for 15 km for north–south nodal plane

Focal depths (km)	10	15	20	25	30	35
Variance	0.1856	0.1958	0.1981	0.2065	0.2094	0.2207
Mw	7.59	7.61	7.60	7.66	7.65	7.68

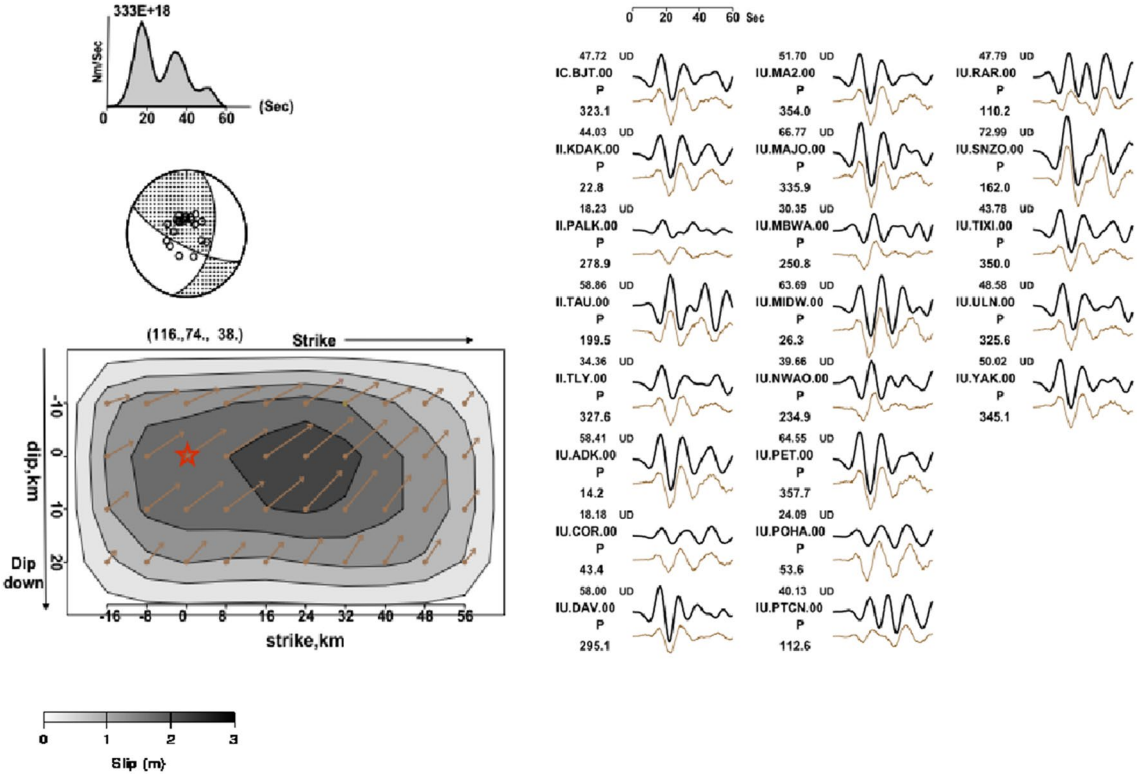

Fig. 3 Teleseismic waveform inversion result for the Mw 7.6 on April 12, 2014, for the east–west nodal plane. The red star indicates the hypocenter set at a depth of 15 km and the arrows show the direction of the fault slip. On the left is the source time function, focal mechanism, and slip distribution. On the right are the observed (bold lines) and model (thin brown lines) waveform data

From the aftershock distribution, it is not clear which of the two nodal planes is the fault plane so, we tested both the north-dipping plane with a strike angle of 279° and dip angle of 46° and the south-dipping plane with a striking angle of 104° and dip angle of 44° for the assumed fault planes. The size of the fault plane is 56×56 km with a subfault size of 8×8 km. The epicenter was fixed at 11.463°S 162.051°E with a hypocentral depth of 35 km. Similar to the Mw 7.6 event, we tested several hypocenter depths and Table 3 shows the variances for the north-dipping plane using for different depths, including the smoothing. The optimal hypocentral depth was determined to be 35 km. The south-dipping plane also showed a similar optimal depth near 30 km depth. Like the Mw 7.6 event, the inversion results are not very sensitive to the assumed epicenter. The results are also not sensitive to the assumed rupture velocity and a value of 2.5 km/s was used.

Figures 5 and 6 show the slip distribution that was determined for the north-dipping and south-dipping nodal planes, respectively. The slip distributions are contained at distances of 56 km in both the strike and dip directions. The pattern of slip for the north dipping plane (Fig. 5) shows a simple pattern with a maximum displacement of about 2 m located west and slightly shallower than the hypocenter. The seismic moment is 1.57×10^{20}Nm, which corresponds to Mw 7.4. The south-dipping plane (Fig. 6) shows a more complicated distribution of slip with a maximum displacement of about 2 m located east and slightly deeper than the hypocenter. The seismic moment is 1.56×10^{20}Nm, also corresponding to Mw 7.4. The simpler slip distribution for the north dipping plane suggests that this is likely the fault plane for the earthquake. Using different values for the depth of the hypocenter does not significantly change the patterns of slip distribution. Our hypocentral depth is slightly different from the USGS depth, although the difference is smaller than the vertical grid size used in our inversion.

USGS assumed the south-dipping plane was the fault plane and shows a slip distribution (https://earthquake.usgs.gov/earthquakes/eventpage/usc000piqj/finite-fault). The slip distribution is somewhat similar to our solution with areas of large slip both above and below the hypocenter. Although in the USGS solution the area above has a larger slip amplitude while in our solution the area below has a larger amplitude. If this is not the correct fault plane, the solution may be more unstable, and small

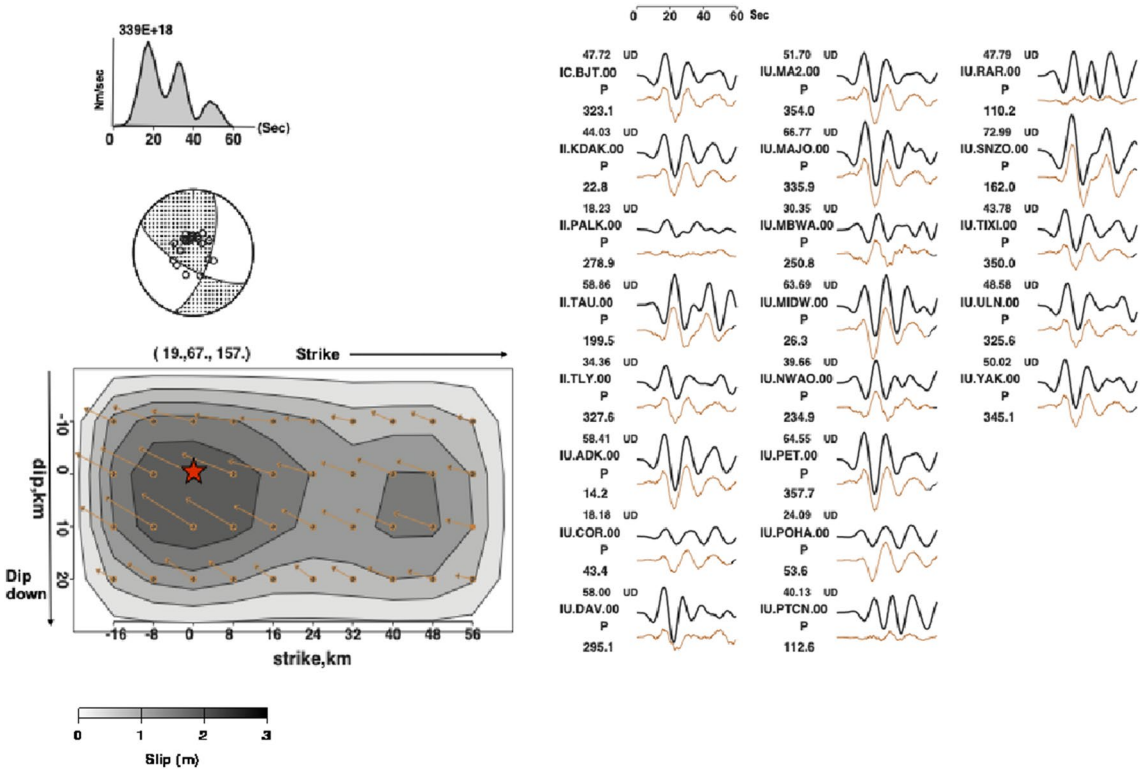

Fig. 4 Teleseismic waveform inversion result for the Mw 7.6 on April 12, 2014 for the north–south nodal plane. The red star indicates the hypocenter set at a depth of 15 km and the arrows show the direction of the fault slip. On the left is the source time function, focal mechanism, and slip distribution. On the right are the observed (bold lines) and model (thin lines) waveform data

Table 3 Testing of various starting hypocentral depths from 20 to 45 km for the north dipping plane of the Mw 7.4 earthquake

Focal depths (km)	20	25	30	35	40	45
Variance	0.2335	0.2107	0.1917	0.1810	0.1811	0.1818
Mw	7.33	7.38	7.40	7.44	7.48	7.52

The optimal hypocentral depth was 35 km

differences in station distribution and data selection may affect the estimated slip distribution.

Static Coulomb stress changes

Using the slip model for the Mw 7.6 earthquake on April 12, we calculated the static stress changes in the region of the Mw 7.4 event on April 13 for the orientations of the two possible fault planes. The program DC3D by Okada (1992) is used to determine the displacement for any point in the half-space medium for a dislocation on a fault plane, assuming that the Earth is an elastic half-space. We then calculate the shear stress change, $\Delta\tau_s$, and normal stress change, $\Delta\sigma_n$, for the assumed orientation. The results are shown in terms of the Coulomb Failure Criterion (ΔCFF):

$$\Delta \mathrm{CFF} = \Delta\tau_s + \mu\prime\Delta\sigma_n, \quad (1)$$

where μ′ is the apparent friction coefficient with a value of 0.4. The results for the static Coulomb stress changes (ΔCFF) are shown in Figs. 7 and 8, assuming a north-dipping and south-dipping fault plane, respectively.

The black rectangles show the surface projections of the fault planes for the two events. Since the ΔCFF depends on the depth, the stress calculations were done for four depths from 25 to 40 km, which corresponds to the depths of the fault plane for the Mw 7.4 earthquake. The red/blue areas correspond to areas of positive/negative stress changes for triggering an earthquake. In Fig. 7, assuming a north-dipping plane, for all depths, the entire fault area of the April 13 event is in a positive

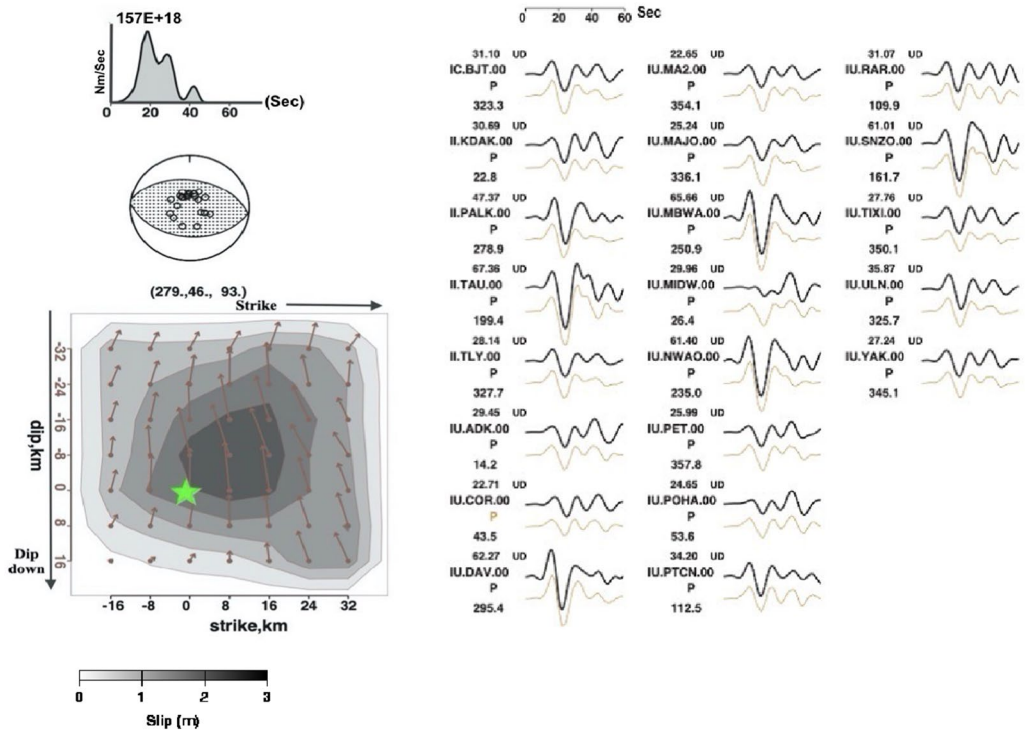

Fig. 5 Teleseismic waveform inversion results for the north dipping fault plane of the Mw 7.4 event on April 13, 2014. The green star indicates the hypocenter at 35 km. On the left are the source time function, focal mechanism and slip distribution. On the right are the observed (bold lines) and model (thin brown lines) waveform data

(red) area. The maximum amount of stress increases near the hypocenter of the Mw 7.4 event is 48.6 kPa at a depth of 15 km. In Fig. 8, assuming the south-dipping fault plane, for all depths most of the area of the fault for the Mw7.4 event is in an area of positive (red) stress change, although some of the areas on the northern up dip edge are in negative (blue) regions. The value of the stress increases near the hypocenter for the Mw 7.4 event is 18.3 kPa at a depth of 35 km, Fig. 8c. From these results of the static stress changes, there are calculated positive stress changes for almost the entire fault area of the M7.4 event, considering both cases of a fault plane that is north-dipping or the south-dipping. For the preferred north-dipping fault plane the increase of static stress is larger than for the south-dipping south plane.

For triggering earthquakes, it is difficult to know what is the minimum level of stress change needed. However, it is generally thought that stresses have to be larger than those caused by Earth tides, because tidal triggering does not seem to be common. Stein (1999) shows fairly clear increases of seismicity on active faults due to stress changes of about 10 kPa. The calculated static stress changes in this study are larger than this threshold.

Aftershock rates

The modified Omori's law (Omori 1895; Utsu 1961, 1966) describes the rate of aftershocks following a mainshock:

$$n(t) = K/(t+c)^p, \tag{2}$$

where n is the rate of aftershocks, t is the time, and K, c, and p are empirical constants determined for the specific sequence. The p-value is the decay rate of an aftershock sequence, which gives the rate of a power law decay curve. We use this formula to calculate the aftershock rate during the time between the Mw 7.6 and Mw 7.4 earthquakes. We computed maximum likelihood estimates of the K, c, and p parameters. The parameter estimation is done for aftershocks during the 12 h following the Mw 7.6 event which is before the occurrence of the Mw 7.4 event. We used aftershocks with mb equal to or larger than the completeness level of 4.0 (USGS). We estimated $K=68$, $c=0.08$ day, and $p=1.01$. In Fig. 9, the observed cumulative number of aftershocks (black line) is compared to the predicted number determined from the 12 h of data (red line). Note that there is a strong increase of seismicity above the predicted rate starting about 5 h before the occurrence of the Mw 7.4 earthquake. These might be 'foreshocks' to the Mw 7.4 event and show that there was a significant increase in seismic

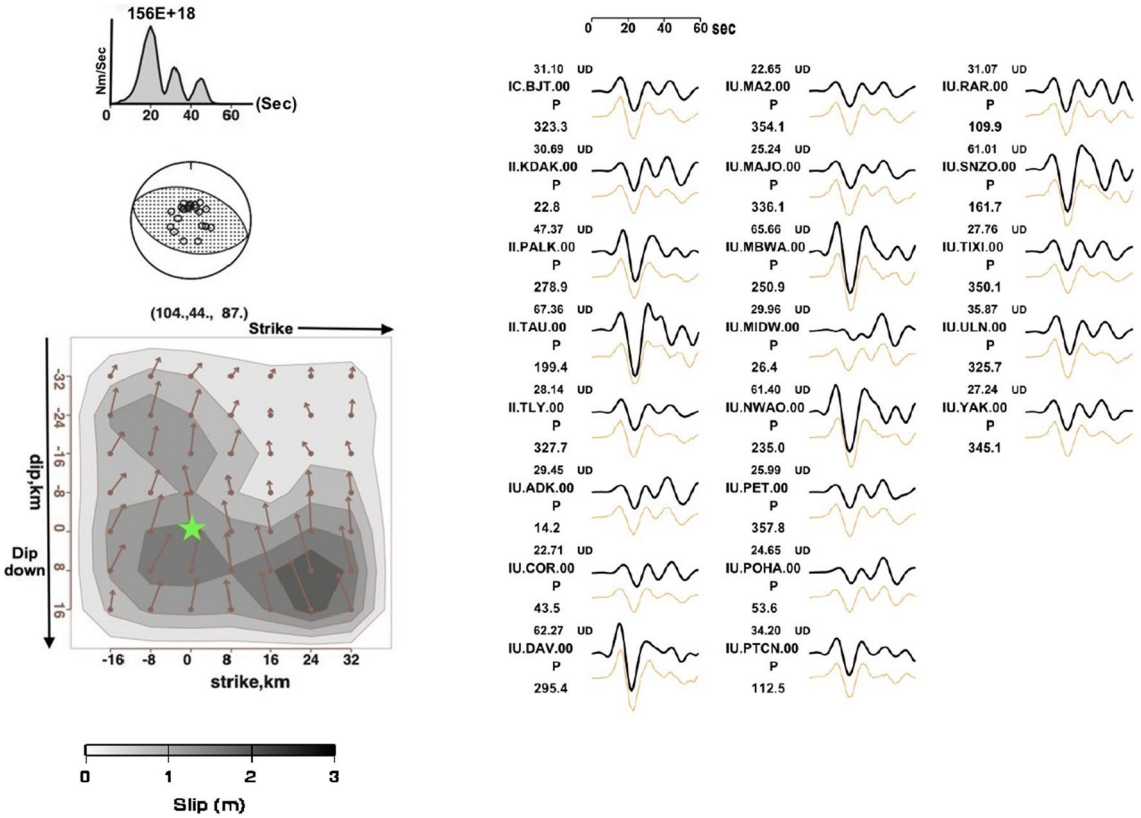

Fig. 6 Teleseismic waveform inversion results for the south-dipping fault plane of the Mw 7.4 event on April 13. The green star indicates the hypocenter at 30 km. On the left are the source time function, focal mechanism and slip distribution. On the right are the observed (bold lines) and model (thin brown lines) waveform data

activity leading up to the triggering of the Mw 7.4 earthquake. This increase is not due to a secondary aftershock sequence because there are no large aftershocks at this time. The rate increase is comparable to the increase of aftershocks following the Mw7.4 event, so if the increase was a secondary aftershock sequence, it would require an event around M7 or larger.

Figure 10 shows the spatial distribution of aftershocks for 20 h following the Mw 7.6 event, which includes several hours after the Mw 7.4 event. It is observed that a few hours after the Mw 7.4 event (15–17 h after the M7.6 event) the aftershocks concentration does not deviate greatly from the NW–SE distribution pattern observed after the Mw 7.6 first event. The aftershock activity following the Mw 7.6 event may also increase the stress field around the hypocenter of the Mw 7.4 event, contributing to the triggering, as proposed by Yamamoto et al. (2002) and Felzer (2004), as will be discussed in the next section.

Discussion

Our results show that the Mw 7.4 earthquake was likely triggered by static stress changes caused by the Mw 7.6 earthquake, which occurred about 16 h earlier. This sequence and other multiple events in the region may be related to the complex geological structures that may be conducive to earthquake triggering. (e.g., Pollitz and Johnston 2006).

The 2014 sequence of earthquakes is generally consistent with an asperity model that was proposed for the frequent doublet earthquake characteristic of the Solomon region by Lay and Kanamori (1980). Their model explains that the stress distribution of the Solomon Islands region is due to the rapid convergence rate that produces the short recurrence time and rapid strain accumulation in the region with relatively small size asperities. This stress accumulation promotes a doublet type of failure for the region, where the failure of one asperity can trigger slips on a nearby asperity of similar size that is also highly stressed, producing another similar size earthquake. This asperity model mainly explains earthquake doublets for large plate boundary events on the subduction interface. However, the sequence in 2014 is somewhat different

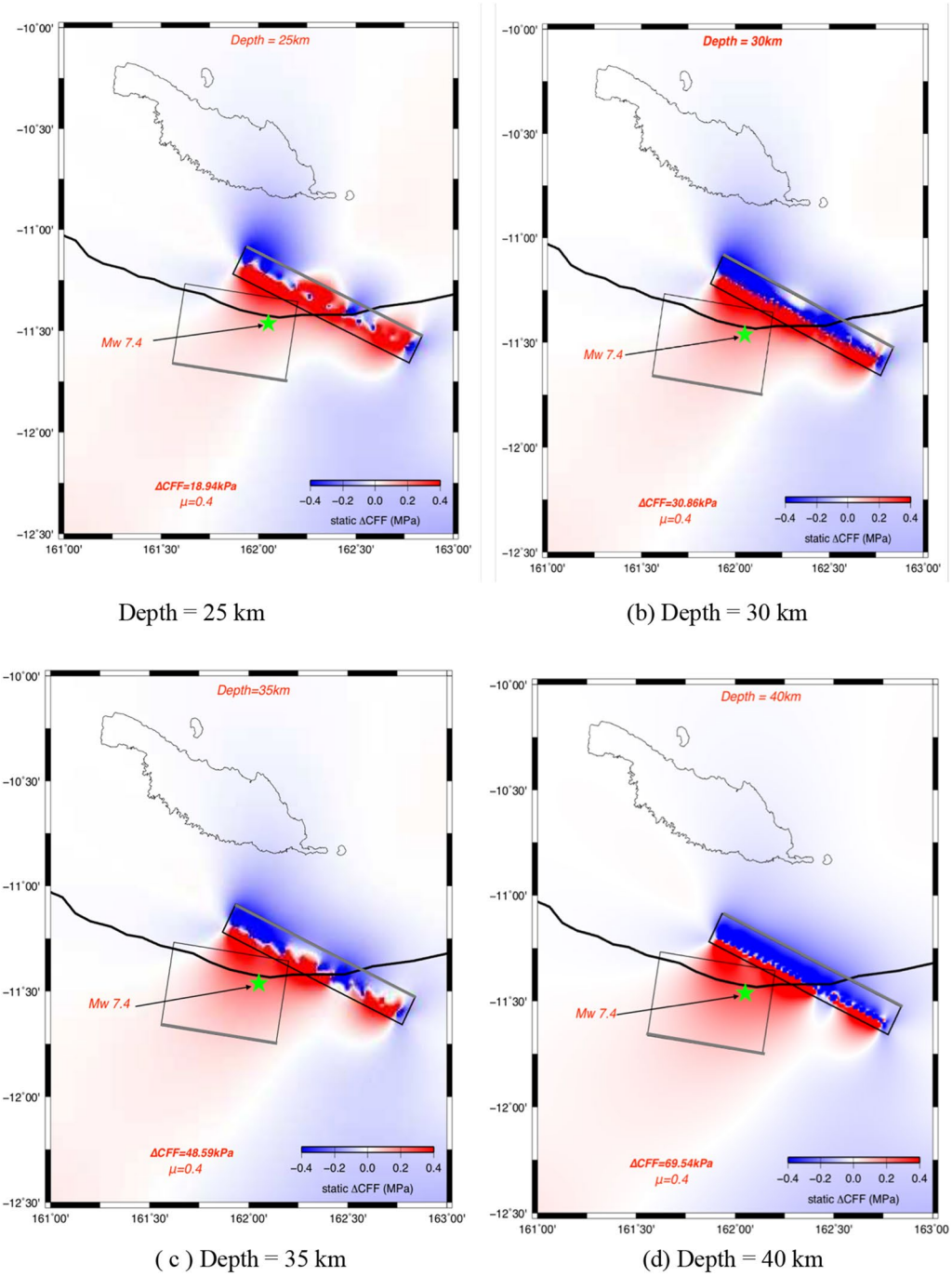

Fig. 7 Static stress changes from Mw 7.6 event for north dipping plane of the Mw 7.4 event**.** Star indicates the epicenter of the Mw 7.4 event. The narrow rectangle panel is the surface projection of the fault plane of Mw 7.6 event and the wider rectangle is the Mw 7.4 north dipping fault plane. The thicker line of the rectangles shows the upper edge of the dipping planes. **a**–**d** are the static stress changes for different depths and all depths show a strong increase around the hypocenter of the Mw 7.4 event

from the Lay and Kanamori model because the first Mw 7.6 earthquake is a plate boundary earthquake, but the 2nd Mw 7.4 earthquake is an intraplate event within the subducting slab.

To discuss intraplate/interplate earthquakes in 2014, we propose an extension to the model of Lay and Kanamori. Figure 11 shows a configuration of closely spaced asperities that may not be limited to the interplate interface,

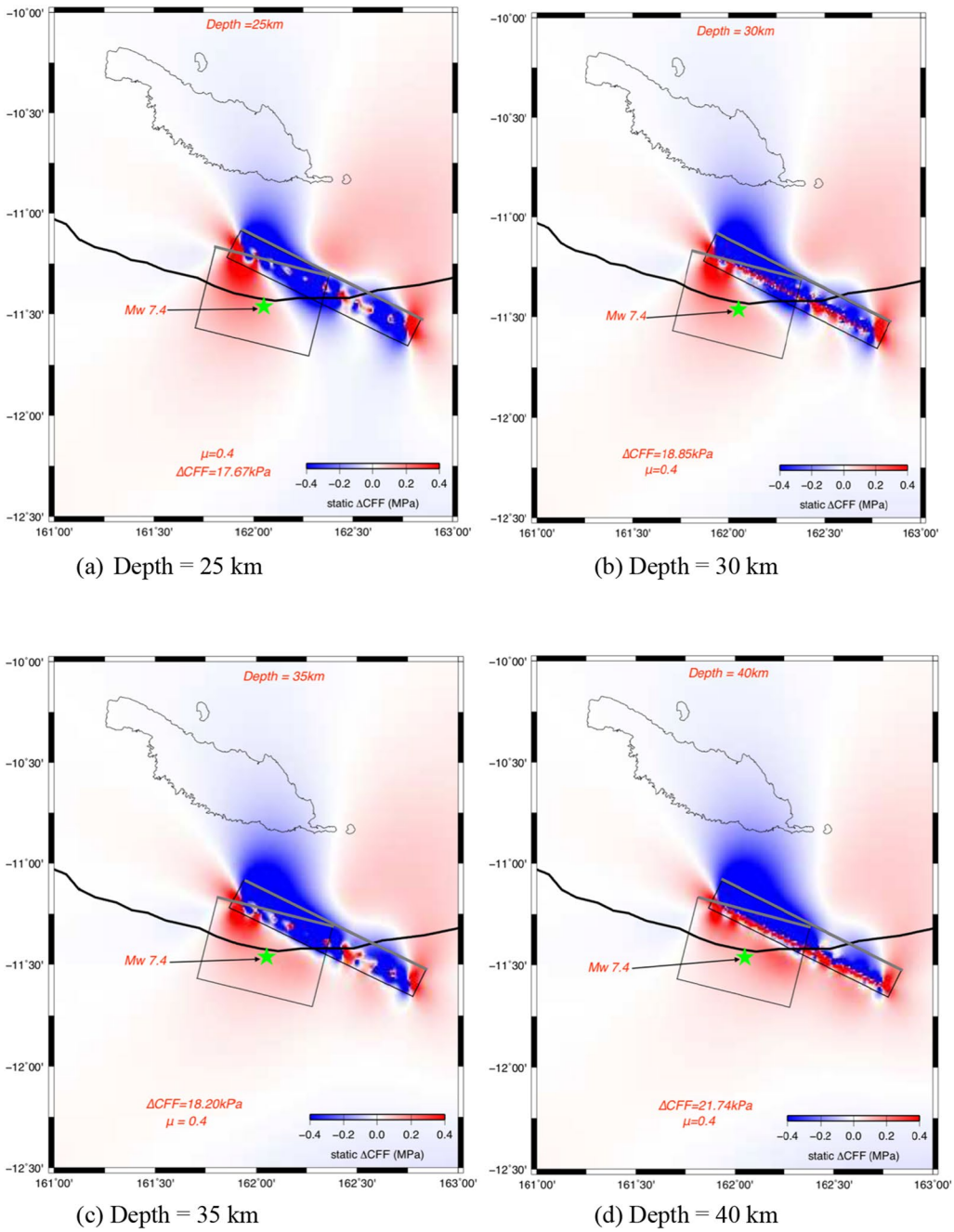

Fig. 8 Static stress changes from Mw 7.6 event for south-dipping plane of the Mw 7.4 event. Star indicates the epicenter of the Mw 7.4 event. The narrow rectangle is the surface projection of the fault plane of the main event and wider rectangle is the Mw 7.4 south-dipping fault plane. The thicker line of the rectangles shows the upper edge of the dipping planes (**a**–**d**) show different depths for the static stress changes and indicate there was an increase of stress around the hypocenter of Mw 7.4 event

but include both interplate and intraplate regions. The very complicated geologic structure in the Solomon Islands may produce highly stressed patches that exist close together but not necessarily only on the subduction interface. These closely spaced asperities are distributed throughout the region and will promote the triggering of earthquake doublets between both interplate and intraplate regions.

Yamamoto et al. (2002) and Felzer (2004) proposed an alternative explanation for the frequent doublet earthquakes in the Solomon Islands region after they observed a similar doublet in the Ometepec, Guerrero area of

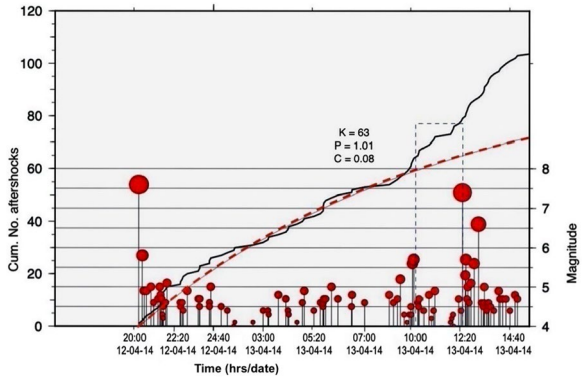

Fig. 9 The temporal distribution of aftershocks during the 20 h following the Mw 7.6 earthquake, which includes the time of the Mw 7.4. event at 12:36. Observed cumulated number of aftershocks (black line) and predicted number determined from the modified Omori law using data of the first 12 h (red line) are shown. The dotted box shows the time of increased activity before the Mw 7.4 event

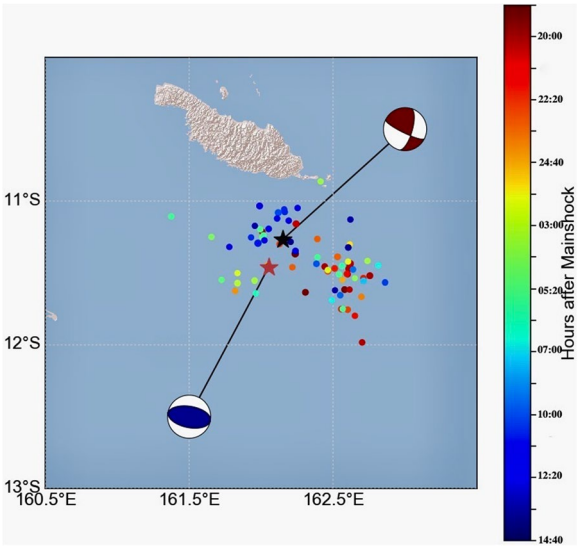

Fig. 10 The spatial and temporal distribution of aftershocks for 20 h after the Mw 7.6 event including 4 h after the Mw 7.4 event. The black star indicates the epicenter for Mw 7.6 (red beachball mechanism) and red star is the Mw 7.4 hypocenter (blue beachball mechanism). The colors of the aftershocks indicate the time occurrence according to the color scale on the right

southern Mexico. They reported that a discontinuity in the spatial distribution of aftershocks of a doublet may be related to a structural segmentation of the continental margin crust and the upper part of the descending oceanic plate and contributes to the frequent earthquake doublet occurrence in the area. They suggested that Solomon Islands' multiplets or doublets may be explained simply by a high regional aftershock rate and earthquake density. The 12 h of aftershocks before the Mw 7.4 could be consistent with this aftershock intensity model, especially the increased aftershocks observed 5 h before the occurrence of Mw 7.4. The aftershock distribution

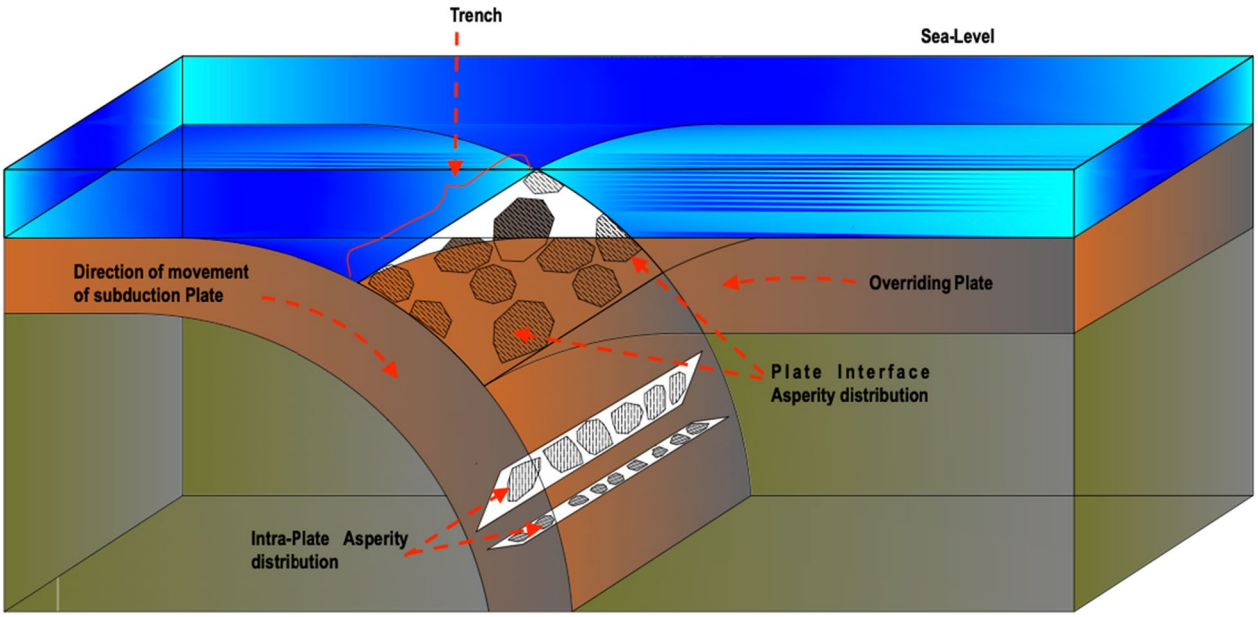

Fig. 11 Interpretative model that shows asperities can occur on the plate interface (plate interface asperity distribution) and on faults within the subducting plate (intraplate asperity distribution). For the 2014 doublet, the Mw7.6 event was on the plate interface and the Mw7.4 event was an intraplate earthquake within the subducting slab

extends mainly along the northwest to the southeast trend of the San Cristobal terrain.

These two proposed explanations (asperity distribution or high aftershock rate) for the doublet earthquakes in the region may be related to similar physical mechanisms. The high aftershock rates discussed by Felzer (2004) and Yamamoto et al. (2002) may be related to the asperity distribution proposed in Lay and Kanamori (1980) and both observations lead to the frequent occurrence of doublet earthquakes. The common occurrence of earthquake doublets in the Solomon Islands region could be a manifestation of the complex geological-tectonic structure of the region, as suggested by Petterson et al. (1999). They suggest that the region is discretized into sections, creating a complex collage of crustal units that results in complex micro-tectonic plates, and complex tectonic structure units, which could advance and trap heterogeneous stress in small sections. This idea might be similar to what Lay and Kanamori (1980) observed and referred to as areas of higher stress (asperities). The regions of higher stress have a distribution of similar-sized discrete zones of higher stress that could trigger multiple earthquakes.

Conclusions

On April 12, 2014, a large (Mw 7.6) strike-slip earthquake occurred along the plate boundary between the Indo-Australia plate and Pacific plate in the Solomon Islands and was followed 16 h later on April 13 by a Mw 7.4 event located approximately 110 km southwest of the epicenter of the Mw 7.6 event. The Mw 7.6 earthquake was a strike-slip event on a fault striking nearly east–west. The April 13, Mw 7.4 earthquake was a thrust event with north- and south-dipping nodal planes. We prefer the north-dipping plane, but there is not a clear trend in the observed aftershock distribution so there is uncertainty in choosing the fault plane. Slip models were estimated for the two earthquakes and these were used to estimate the static stress change from the April 12, Mw 7.6 event on the region of the April 13, Mw 7.4 event. There was a significant increase of static stress (about 20–50 kPa) in the hypocentral region and most of the area of the fault plane for the April 13 event which probably contributed to the triggering of the second event. The aftershock activity generally follows the Omori-Utsu decay law, however, we found an increase in activity 5 h before the occurrence of the Mw 7.4 event. This increase may also be related to the subsequent triggering of the Mw 7.4 earthquake.

Acknowledgement

The Kanamori and Kikuchi (1983) inversion program and the Okada (1985) program for calculation of stress on the fault model are classified as open source programs. Some of these figures were made using the General Mapping Tool (GMT) software (Wessel and Smith 1998).

Author contributions

This manuscript is based on the first author's work for his Masters degree. The research of this study and text of the paper were done by the first author under the supervision of the second and the third authors. All authors read and approved the final manuscript.

Availability of data and materials

The waveform and hypocenter data in this study are in the public domain and were retrieved from the IRIS and USGS websites during March 2019. https://www.iris.edu/hq/ and https://earthquake.usgs.gov/earthquakes.

Declarations

Competing interests

None of the authors have any financial interest or any competing interest related to this manuscript. This research nevertheless was partially funded and supported by the graduate school of science of Kyoto University and partially supported by JAPANESE GOVERNMENT (MONBUKAGAKUSHO SCHOLARSHIP, MEXT).

Author details

[1]Kyoto Sentan Kagaku Daigaku Mukaijima, Graduate School of Engineering, Kyoto, Japan. [2]Kyoto University, Kyoto, Japan.

Received: 22 January 2023 Accepted: 29 April 2023
Published online: 19 June 2023

References

Ekström G, Nettles M, Dziewoński AM (2012) The global CMT project 2004–2010: centroid-moment tensors for 13,017 earthquakes. Phys Earth Planet Inter 200–201:1–9. https://doi.org/10.1016/j.pepi.2012.04.002

Felzer KR (2004) A common origin for aftershocks, foreshocks, and multiplets. Bull Seismol Soc Am 94(1):88–98. https://doi.org/10.1785/012003069

Kanamori H, Kikuchi M (1983) A simple method for seismological inversion of teleseismic body waves for focal mechanism of local earthquake. J Geophys Res 88(B4):3247–3251

Kennett BLN, Engdahl ER (1991) Traveltimes for global earthquake location and phase identification. Geophys J Int 105(2):429–465. https://doi.org/10.1111/j.1365-246X.1991.tb06724.x

Kikuchi M, Kanamori H (1991) Inversion of complex body waves—III. Bull Seismol Soc Am 81(6):2335–2350

Lay T, Kanamori H (1980) Earthquake doublets in the Solomon Islands. Phys Earth Planet Inter 21(4):283–304. https://doi.org/10.1016/0031-9201(80)90134-X

Okada Y (1985) Surface deformation due to shear and tensile faults in a half-space. Bull Seismol Soc Am 75:1135–1154. https://doi.org/10.1785/BSSA0750041135

Okada Y (1992) Internal deformation due to shear and tensile faults in a half-space. Bull Seismol Soc Am 82(2):1018–1040. https://doi.org/10.1785/BSSA0820021018

Omori F (1895) On the after-shocks of earthquakes. J Coll Sci Imp Uni. https://doi.org/10.15083/00037562

Park S-C, Mori J (2007) Triggering of earthquakes during the 2000 Papua New Guinea earthquake sequence. J Geophys Res 112(B3):B03302. https://doi.org/10.1029/2006JB004480

Petterson MG, Babbs T, Neal CR et al (1999) Geological–tectonic framework of Solomon Islands, SW Pacific: crustal accretion and growth within an intra-oceanic setting. Tectonophysics 301(1–2):35–60. https://doi.org/10.1016/S0040-1951(98)00214-5

Poiata N, Koketsu K, Miyake H (2010) Source processes of the 2009 Irian Jaya, Indonesia, earthquake doublet. Earth Planet Sp 62(5):475–481. https://doi.org/10.5047/eps.2010.02.008

Pollitz FF, Johnston MJS (2006) Direct test of static stress versus dynamic stress triggering of aftershocks. Geophys Res Lett 33(15):L15318

Schwartz SY, et al. (1989) Source process of the great 1971 Solomon Islands doublets. Phys Earth Planet Inter 56:294–310. https://doi.org/10.1016/0031-9201(89)90164-7
Stein RS (1999) The role of stress transfer in earthquake occurrence. Nature 402(6762):605–609. https://doi.org/10.1038/45144
Utsu T (1961) A statistical study on the occurrence of aftershocks. Geophys Magazine 30:521–605
Utsu T (1966) A statistical significance test of the difference in b-value between two earthquake groups. J Phys Earth 14(2):37–40. https://doi.org/10.4294/jpe1952.14.37
Wesnousky SG, Astiz L, Kanamori H (1986) Earthquake multiplets in the southeastern Solomon Islands. Phys Earth Planet Inter 44(4):304–318. https://doi.org/10.1016/0031-9201(86)90058-0
Wessel P, Smith WHF (1998) New, improved version of generic mapping tools released. EOS Trans Am Geophys Union 79(47):579-579. https://doi.org/10.1029/98EO00426
Xu Z, Schwartz SY (1993) Large earthquake doublets and fault plane heterogeneity in the northern Solomon Islands subduction zone. PAGEOPH 140(2):365–390. https://doi.org/10.1007/BF00879412
Yamamoto J, Quintanar L, Jiménez Z (2002) Why earthquake doublets in the Ometepec, Guerrero, Mexico subduction area? Phys Earth Planet Inter 132(1–3):131–139. https://doi.org/10.1016/S0031-9201(02)00048-1

Websites

Kikuchi M, Kanamori H Note on Teleseismic Body-Wave Inversion Program, http://www.eri.u-tokyo.ac.jp/ETAL/KIKUCHI/
U.S. Geological Survey, 2017, Earthquake Facts and Statistics, accessed March 22, 2018, at URL https://earthquake.usgs.gov/earthquakes/browse/stats.php
U.S. Geological Survey, 2018, Mineral Resources Data System: U.S. Geological Survey database available online at https://mrdata.usgs.gov/. (Accessed May 14, 2018)
The facilities of IRIS Data Services, and specifically the IRIS Data Management Center, were used for access to waveforms, related metadata, and/or derived products used in this study. IRIS Data Services are funded through the Seismological Facilities for the Advancement of Geoscience and Earth Scope (SAGE) Proposal of the National Science Foundation under Cooperative Agreement EAR1261681
Baker CB, Eischeid JK, Karl TR, Diaz HF (1994) The quality control of long-term climatological data using objective data analysis. Preprints of AMS Ninth Conference on Applied Climatology, Dallas, TX, January 15–20, 1995
The Catalogue data are from the Global Centroid-Moment Tensor (http://www.globalcmt.org)

Publisher's Note